A User- and Slope-Adaptive Control Framework for a Walking Aid Robot

Younggeol Cho ⓘ, Marta Lorenzini ⓘ, *Member, IEEE*, Andrea Fortuna ⓘ, *Graduate Student Member, IEEE*, Mattia Leonori ⓘ, and Arash Ajoudani ⓘ, *Member, IEEE*

Abstract—Walking aid robots have been developed for elderly people or patients facing difficulties while walking. However, most of them are designed only for flat ground, must rely on handles, and have drawbacks such as oscillation and lack of stability. The primary goal of this research is to improve the transparency and safety of a walking aid robot, addressing both flat and sloping terrains. To achieve this goal, we propose a novel variable admittance control strategy for an omnidirectional mobile platform by combining human motion recognition and a slope-adaptive approach. We design a vision system with a wide-angle camera to capture skeletal whole-body information at a close distance to recognize the walking direction. Accordingly, the damping values of the admittance controller are varied. In addition, these parameters are varied with respect to the slope angle of the ground, which is detected by the platform. We validated the controller performance with eleven healthy subjects performing two experiments on both flat and sloping terrains. Three admittance controllers are compared, with fixed parameters, variable damping by Cartesian velocity, and variable damping by walking direction. Experimental results show the advantages of the variable admittance control based on walking direction, which ensures high transparency and smoothness on both flat and sloping terrains.

Index Terms—Walking assistive robot, variable admittance control, slope adaptive control, human motion recognition.

I. INTRODUCTION

RESTORING and supporting walking pose significant challenges, particularly among older adults and people with neurological disorders [1]. Individuals with such limitations face challenges in aligning their actions with their intentions, often requiring external support. This dependency limits their ability to live independently and consequently impacts their overall well-being. In light of this, research efforts in the field of walking assistive technology have been advanced to restore gait functionality and enhance gait stability in rehabilitative and assistive contexts [2], [3]. Various walking assistive robotic platforms exist, categorized by human-machine interface design, movement intention recognition, and device control strategies. One notable example is the smart walker [4], featuring two handles programmed to maintain a set distance from the user. Alternatively, the smart rollator [5] utilizes force sensors on handles to adjust assistance based on interaction. Cane-type assistive robots, like the one in [6], allow single-handed use. For instance, the tool in [7] employs force/torque and distance measurements for robot positioning, fall detection, and balance restoration. However, these platforms primarily rely on upper-body functions for support and safety, limiting accessibility to a narrower range of users. An alternative walking aid configuration involves a rigid harness attached to the user's back [8]. This device operates using interaction force/torque on the coupling part. Additionally, a commercialized walking assistive platform (Andago, Hocoma) has been developed for gait and balance training [9]. These body-coupled assistive devices offer advantages such as partial body weight support (BWS), freedom to use hands, and intuitive platform control.

As concerns control strategies, researchers mostly focused on making the assistive devices follow humans with high transparency. The authors of [4] introduced a control approach based on inverse kinematics, utilizing geometric information from both the human legs and the robot to maintain a precise distance and angle between them. An alternative methodology involved the utilization of admittance controllers, employing diverse sensors positioned at various locations. In [10], a force/torque sensor was attached to the handle of a cane-type robot, and the measured force was employed to generate the robot's desired velocity. This approach also addresses fall prevention and balance by considering the user's center of pressure (COP) [7]. Human motion detection plays a crucial role in enhancing walking assistance capability, particularly for safety measures such as fall prevention and detecting mismatches in human-robot movement that could lead to unsafe situations. In [11], admittance control is merged with quadratic optimization theory to determine appropriate assistive forces and prevent falling based on the zero moment point (ZMP). Additionally, [12] highlights the importance of posture estimation in recognizing abnormal walking postures and assisting humans in unsafe situations. In a recent contribution [8], the authors introduced an omnidirectional assistive platform to be coupled with the user's back. The measured interaction forces are employed for the admittance controller, enabling users to intuitively maneuver the robot and achieve normal speed gait. Similarly in [13] and through a mobile robotic platform, the authors introduced two reactive control modalities based on the COP trajectories to regain balance.

The aforementioned studies have contributed to enhancing the transparency and safety of assistive robots. However, three key

limitations must be addressed. Firstly, these studies employed fixed parameters within the controller for individual users, thereby constraining the performance of the robotic assistant. Researchers have explored the application of variable parameters in the domain of manipulators. For instance, variation strategies in admittance controllers have been investigated to enhance the performance of human-robot interaction [14]. Similarly, the performance of assistive robots can be significantly enhanced by incorporating variable parameters into the controller based on machine learning techniques to adapt to various human physical parameters and walking behavior. In a related approach, a control strategy based on reinforcement learning was proposed, dynamically adapting control parameters according to the user's walking style [15]. Similarly, in a study detailed by [16], model-based reinforcement learning (MBRL) was utilized to fine-tune the control policy of the robotic assistant, facilitating coupled human-robot motion in a front-following scenario. This method demonstrated reduced movement jerk and enhanced task execution speed while ensuring safety. However, it was applied within a weak coupling type of assistive robot system with humans, and it required a considerable amount of data and computational resources.

The second concern pertains to oscillation, which is inevitable in robot-human interactions when the coupling is rigid. While this coupling offers advantages such as intuitive control and rapid safety response, we aimed to demonstrate that observation of the human body by vision and variation of parameters can mitigate oscillation. Previous efforts to address oscillations have involved methods such as integer order admittance controllers [17] or optimizing controller parameters [8]. However, these approaches haven't provided an ultimate solution, often resulting in challenges such as time delays and diminished robot transparency. We are working on analyzing and minimizing oscillations from both hardware and control perspectives.

The third challenge involves the adaptability and stability of assistive robots on sloping ground. Prior research addressed this by applying gravity cancellation into the controller for sloping ground adaptation [18]. Another study compensates for gravity by modulating force input in response to the slope degree [19]. In these studies, the ability of users to maneuver the robot on sloping ground was improved, making it similar to flat ground. However, these studies focused only on the handle type of assistive walker, and the user's weight was estimated roughly using a potential meter attached to the part connected to the handler thus leading to inaccuracies.

In this paper, We propose a novel approach to monitor the human body using a camera and control a robot intuitively with an admittance controller. Our focus is on improving transparency and movement smoothness, demonstrating that variable admittance control via walking direction recognition significantly enhances these aspects. We highlight our method of varying the damping parameter in each direction, utilizing damping variation curves tailored to walking velocity. Additionally, we developed a slope-adaptive function that relies on working direction recognition, aiming to enhance the mobility and stability of the assistive platform. To the best of our knowledge, this innovative approach integrates vision-based walking direction recognition with a controller for walking assistive robots, thereby enhancing walking performance and safety on sloping terrain. This research has the potential for a range of applications including fall prevention, balance recovery, and rehabilitation therapy.

II. METHODOLOGY

We describe our hardware and control framework through three components in this section. A. walking Assistive omNi-Directional Exo-Robot (WANDER), B. skeletal feature extraction and walking direction recognition, C. variable admittance control strategy on the flat ground, and D. slope adaptive variable admittance control strategy (see Fig. 1).

A. Walking Assistive Omni-Directional Exo-Robot (WANDER)

In this section, we offer a concise overview of the Walking Assistive omni-Directional Exo-Robot (WANDER) developed by our group, depicted in Fig. 2(a). WANDER. The driving base of WANDER is a SUMMIT-XL STEEL MOBILE ROBOT from Robotnik Co. An aluminum structure was constructed atop it to support the user's weight and accommodate sensors. The primary objective of WANDER is to follow and support users during walking, with a maximum required velocity set below 1.5 m/s, considering typical walking speeds around 1.0 m/s [20]. WANDER's physical dimensions are 978 mm x 776 mm x 510 mm, weighing 105 kilograms, with a payload capacity of 250 kilograms. The human and WANDER were rigidly coupled through a lumbar brace at the level of the low back, equipped with a 6-axis force/torque (F/T) sensor (LaxOne, BotaSystems Co.). This coupling interface allows for measuring the interaction forces and torques between them. The range of measurement is equal to 4 kN in the direction perpendicular to the torso and 1.8 kN along the others. This range has been determined considering falls, loss of balance, and walking on sloping ground. Its resolution is approximately 300 mN and 400 mN for the respective directions. To capture the whole human body from a close distance (see Fig. 2), considering WANDER's spatial limitations, a wide field of view camera with a short focal length (GoPro HERO11, GoPro) was installed on the aluminum structure. This setup guarantees that the human body can be captured from a distance of less than 50 cm from the back. The image was rectified with the intrinsic parameters of the camera to calibrate the distortion. Furthermore, an inertial measurement unit (IMU) is integrated into WANDER to measure the slope angles during walking.

B. Recognition of Walking Direction Via Human Skeletal Movement Extraction.

Before delving into the methodology, it's valuable to examine human walking patterns in daily life. When transitioning between locations, individuals predominantly walk forward, whether indoors or outdoors, like sidewalks and crosswalks. Turning is also common; individuals typically change direction while walking. Also, when people want to move from one point to another, several paths are possible, but the dominant walking patterns are forward walking and turning (see. Fig. 3(a)). Walking backward and lateral are less common in daily life but may occur in specific situations (see Fig. 3(b)). For example, When pulling an object from the end of a corridor, walking backward may be necessary. When navigating between close walls, people may need to walk laterally. In addition, we don't usually walk diagonally, which is ergonomically inefficient and we just walk with a turn on the curved track. Given all the above considerations, in this paper, we categorized walking directional patterns as standing (S), longitudinal (F: forward
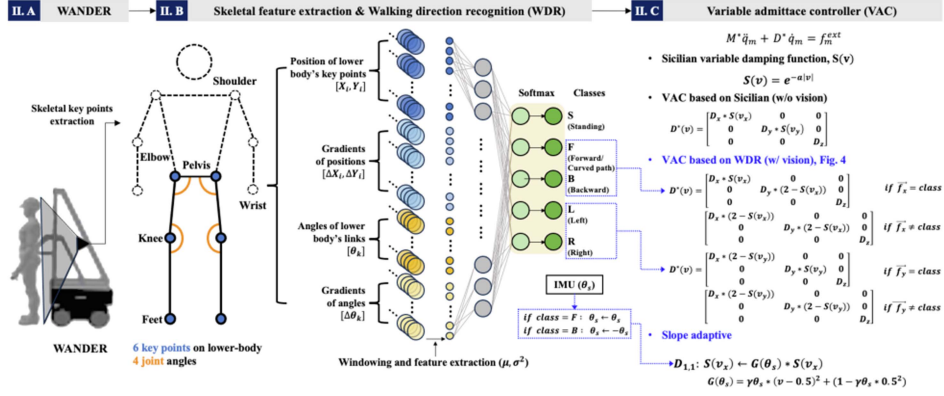
Fig. 1. The WANDER and the proposed control framework. A. Extracting skeletal points and angles. B. Defining and recognizing walking direction features, including key point positions and angles. C. Implementing a variable admittance controller based on walking direction and ground slope angle.
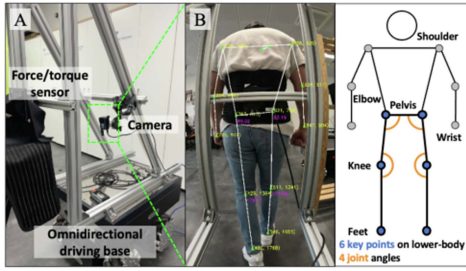

Fig. 2. A. WANDER consists of an omnidirectional driving base plus an aluminum structure, a force/torque (F/T) sensor, an inertial measurement unit (IMU), and a wide-angle camera. B. Human skeletal information was extracted via machine learning-based vision processing.
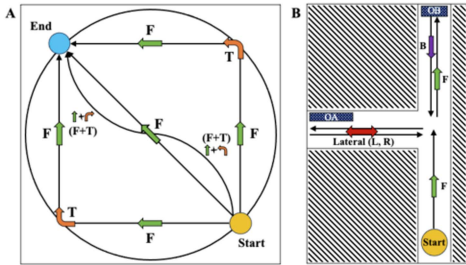

Fig. 3. Walking patterns in daily life. A. From one place to another, even though people have multiple routes, the dominant patterns are forward walking (F) and turning (T). B. People can walk backward (B) and lateral (Left (L), Right (R)) in specific situations.

including walking on the curved track, B: backward), and lateral (L: left, R: right) walking.

To estimate the direction of human movement during walking, a machine learning-based method was developed. First, human skeleton information was extracted from camera images by using the pose detection model Movenet [21], a machine learning-based model that extracts seventeen key points of the human body with over 30 frames per second. Six key points of the lower body were considered for our purpose, i.e., two points from the pelvis, knees, and feet, respectively. The joint angles of the lower body were then computed by using the law of cosines with three points.

Then, a lightweight classification neural network was designed to classify the five distinct walking motions. This network utilizes skeletal information (S) extracted from six key point positions ($[X, Y]$), four lower body angles (θ), and their time derivatives $[dX, dY]$

$$S_t = [[X_t, Y_t],\ \theta_t,\ [dX_t, dY_t],\ d\theta_t]. \qquad (1)$$

The skeletal information was sampled at frequency f, and an N-step window was applied to compute mean and variance values and create a feature $F_t = [\mu_{S_t}, \sigma^2_{S_t}]$, where

$$\mu_{S_t} = \frac{1}{N}\sum_{i=0}^{N} S_{t-i},\ \sigma^2_{S_t} = \frac{\sum_{i=0}^{N}(S_{t-i} - \mu_{S_t})^2}{N-1}. \qquad (2)$$

The classifier comprised an input layer, a single hidden layer, and an output layer (O) with the softmax function (s)

$$O_t = s\left(f_a(W.F_t + B)\right),\ s(x_i) = \frac{\exp(x_i)}{\sum_j \exp(x_i)}. \qquad (3)$$

The hidden layer contained twenty-five nodes, and we used the rectified linear unit (ReLU) as its activation function (f_a). The network propagated with the weight (W) and the bias (B). The classification task encompassed five distinct classes: standing, longitudinal walking (both forward and backward), and lateral walking (both left and right). Loss (L) was defined as

$$L = -\sum_{i=1}^{5} \hat{O}_{t,i} \ln O_{t,i}, \qquad (4)$$

with the true label ($\hat{O}$) by a cross-entropy function. The network was trained by minimizing the loss via Adam optimizer [22].

C. Variable Admittance Control Strategy (VAC) Based on Walking Direction

The user's intention in terms of force/torques that are exerted on the human-robot coupling interface can be translated into desired velocities for WANDER through an admittance controller, making the robot compliant with human motion. The proposed control strategy involves the dynamic adjustment of parameters within the admittance controller based on walking direction recognition presented in Section II-B. This control

strategy primarily aimed to enhance transparency, mitigate oscillations, and thereby improve both assistive performance and safety. The governing equation for the admittance controller can be represented as follows

$$M\ddot{q}_m + D^*\dot{q}_m = f_m^{ext} \tag{5}$$

where M and D^* are the positive definite matrix of mass and damping with only diagonal elements. q_m is the desired position of WANDER, $\dot{q}_m$ and $\ddot{q}_m$ are its velocity and acceleration, and f_m^{ext} is the measured external force from the F/T sensor included in the coupling interface.

1) VAC by Cartesian Velocity (VAC_{vel}): We implemented two types of damping variations within the admittance controller. The first involved modifying the damping based on the Cartesian velocity which is calculated in the admittance controller. To vary damping values, we used a formula ($S(v)$) in previous research [23] that was applied to the variable impedance control for manipulating the robot arm.

$$S(v) = \max\{e^{-\alpha|v|}, S_{\min}\} \tag{6}$$

v represents the Cartesian velocity ($= \dot{q}_m$), which is calculated using 5 with the measured interaction force. We can modulate the interval of damping variation by using index α. $S_{\min}$ is the minimum damping variation ratio. $S(v)$ has an interval $[S_{\min}, 1]$ with respect to v. By using this formula, the damping variation by Cartesian velocity is presented as

$$D^*(v) = \begin{bmatrix} D_x S(v_x) & 0 & 0 \\ 0 & D_y S(v_y) & 0 \\ 0 & 0 & D_z \end{bmatrix} \tag{7}$$

where D^* is a modulated damping matrix. Both D_x and D_y are the initial longitudinal and lateral damping parameters of the admittance controller. D_z is the rotational damping. D_x and D_y vary with v_x and v_y respectively according to (6).

2) VAC Based on Walking Direction (VAC_{WDR}): In addition to Cartesian velocity-based damping variation, we merged it with walking direction recognition (WDR) shown in Section II-B. The basic frame of the damping matrix is similar, but, we used different formulas depending on the walking direction. when the recognized walking direction (C) is longitudinal walking (F, B), the damping matrix varies as

$$D^*(v) =$$
$$\begin{cases} \begin{bmatrix} D_x S(v_x) & 0 & 0 \\ 0 & D_y(2 - S(v_x)) & 0 \\ 0 & 0 & D_z \end{bmatrix}, & \text{if } \overrightarrow{v_x} = C \\ \begin{bmatrix} D_x(2 - S(v_x)) & 0 & 0 \\ 0 & D_y(2 - S(v_x)) & 0 \\ 0 & 0 & D_z \end{bmatrix}, & \text{if } \overrightarrow{v_x} \neq C. \end{cases} \tag{8}$$

The only longitudinal velocity (v_x) is considered. D_x and D_y are varied with respect to v_x for each case of considering the directional match between v_x and recognized walking direction. For instance, when we are walking in a longitudinal direction, the classifier determines whether the movement is 'forward' or 'backward'. In response, we reduce the damping (D^*) values along the longitudinal axis by $S(v_x)$ while increasing them by $(2 - S(v_x))$ along the lateral axis (see (8)). We apply it with the condition that $\overrightarrow{v_x}$ is the same as C. The vector $\overrightarrow{v_x}$ follows
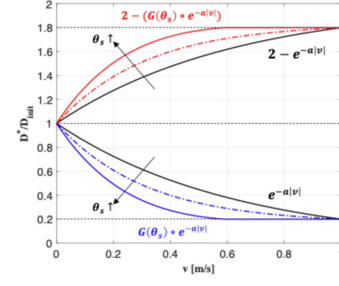

Fig. 4. Variable damping curves by Cartesian velocity and walking direction. The curves blue-side are for decreasing damping when the $\overrightarrow{v}$ is the same as the walking direction. The curves red-side are for increasing damping when the $\overrightarrow{v}$ is opposite or for perpendicular direction. both side curves are also modulated by the slope angle θ_s with the formula $G(\theta_s)$.

a binary condition where positive values signify "forward" and negative values denote "backward" Similarly, $\overrightarrow{v_y}$ operates under the same principle, where positive values represent "right" while negative values represent "left". Other wised, D^* along the both axis are increased. Conversely, when the human walks laterally, the adjustments are opposite, and v_y is only considered as

$$D^*(v) =$$
$$\begin{cases} \begin{bmatrix} D_x(2 - S(v_y)) & 0 & 0 \\ 0 & D_y S(v_y) & 0 \\ 0 & 0 & D_z \end{bmatrix}, & \text{if } \overrightarrow{v_y} = C \\ \begin{bmatrix} D_x(2 - S(v_y)) & 0 & 0 \\ 0 & D_y(2 - S(v_y)) & 0 \\ 0 & 0 & D_z \end{bmatrix}, & \text{if } \overrightarrow{v_y} \neq C. \end{cases} \tag{9}$$

Using (8)–(9), WANDER is expected to show high transparency in the same direction of walking and low oscillation achieved through increasing the damping in the opposite and horizontal directions. The damping variation ratio curves with $S(v)$ are presented in Fig. 4. During periods of standing, we maintained the initial values defined at the experiment's onset for each subject, as explained in the experimental protocol section.

D. Slope Adaptive Variable Admittance Control ($VAC_{WDR,S}$)

To facilitate human walking on slopes, the admittance parameters were adjusted in response to changes in the slope angle of the ground. Otherwise, the perceived human body weight on inclined surfaces will be misinterpreted as pulling or pushing forces depending on the slope, and lead to unsafe robot behaviors (e.g., pushing a user while walking downhill). To confront this, we utilized an IMU sensor with precise Euler angle measurement capabilities and a drift compensation algorithm. An extended Kalman filter was applied, and a barometer was incorporated to compensate for variations due to changes in temperature and pressure affecting the sensor. Based on the angle, we added an additional formula above the variable damping matrix as

$$S(v_x) \leftarrow G(\theta_s)S(v_x) \tag{10}$$
$$G(\theta_s) = \gamma\theta_s(v - 0.5)^2 + (1 - \gamma\theta_s 0.5^2) \tag{11}$$

$$\theta_s = \begin{cases} \theta_s, & \text{if } C = F \\ -\theta_s, & \text{if } C = B \end{cases}. \tag{12}$$

The damping parameters were varied according to the slope angle θ_s with the radian value. This function maintains the D/D_{init} value equivalent to flat ground at zero velocity, while also ensuring minimum and maximum values (min: 0.2, max: 1.8) are upheld at a maximum velocity of 1 m/s. Additionally, it follows a second-order polynomial function $G(\theta_s)$, with a minimum value set based on the primary walking speed set at 0.5 m/s based on Parkinson's disease patients' average gait speed [24]. This control strategy was designed to adjust the admittance parameters to be decreased according to the slope angle of the inclining ground to improve the transparency of WANDER for walking easily. On the other hand, the admittance parameters were increased on the declining ground to ensure stability for users to feel safer. The slope adaptive function ($G(\theta_s)$) adjusts the curve shape based on the slope angle, relying on WDR. The sign of the angle is changed based on walking direction, and the curves of damping variation by the slope angle can be adjusted with the gain γ.

III. EXPERIMENTAL CAMPAIGN

A. Participants

Eleven healthy volunteers (aged 29.2 ± 2.7 years, with a height of 177.0 ± 6.5 cm, and weight 69.4 ± 5.6 kg) were recruited. None of the participants had a history of gait-related diseases. A comprehensive explanation of the experiment and associated precautions was presented, and their informed consent was obtained. The entire experimental process was conducted within the Human-Robot Interfaces and Interaction (HRII) Laboratory at the Istituto Italiano di Tecnologia (IIT), in strict adherence to the principles outlined in the Declaration of Helsinki. The research protocol employed in this study received formal approval from the ethics committee of Azienda Sanitaria Locale (ASL) Genovese N.3, as documented under Protocol IIT_HRII_ERGOLEAN 156/2020.

B. Training Session

To train the proposed model, data were collected from subjects by using the following protocol. Each subject was connected to WANDER by using a lumbar brace at the pelvis level. Prior to the experiment, it was necessary to determine the appropriate parameters (mass, damping) for the admittance controller for each subject. In the [8], they used fixed parameters for all subjects, and authors in [25] set the parameters based on leg motion. However, these methods were for different assistive platforms. Therefore, based on the author's experience with the platform, we set an empirical rule to search initial parameters. Mass (M_x, M_y) for each subject was 115% of the weight and damping (D_x, D_y) was 57.5% (half of 115%). Values of M_z and D_z were fixed as $0.33 \times$ of M and D respectively.

During the training session, the subject walked a squared, spline, and circle track (see Fig. 5). We instructed each subject with simple guidelines regarding walking speed. We suggested that they walk at their normal pace without the robot platform. The average speed of all three controllers across all subjects is similar, approximately around 0.7 m/s. Subjects first stood for ten seconds with shaking movements to improve standing
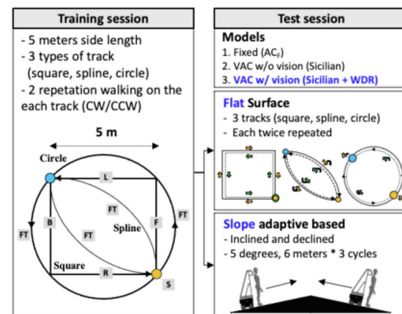

Fig. 5.   Schematic diagram of the experimental protocol.

recognition accuracy. They walked counterclockwise in the forward (F), left (L), backward (B), and right (R) directions on a square track. While walking on the spline and circle tracks, data for forward walking (F) were collected. This sequence was repeated clockwise. Throughout the training, we recorded human skeleton information to extract features. Features were sampled at 30 Hz, and a 0.5-second window was used to compute mean and variance values for each feature. To conduct the training, we utilized 80% of the data, reserving the remaining 20% as test data. The training data was randomly shuffled and divided into batches of 200 samples each, facilitating mini-batch learning. For validating classification accuracy, we used additional data collected in the following test section.

C. Test Session

To validate the performance of the proposed control strategy, we conduct experiments on the flat and sloping ground (see. Fig. 5). Three models were compared: Admittance Control with Fixed parameters (AC_F), VAC by Cartesian velocity (VAC_{vel}), and VAC Based on walking direction recognition (VAC_{WDR}) respectively. The modulation parameters α, $S_{\min}$ were empirically fixed as 0.2 and $ln(0.2)$ respectively for the variation ratio of the damping ($S(v)$) within the interval of [0.2, 1]. γ was also fixed as 20.

1) Flat Ground Experiments: On the flat ground, the subject walked the three types of tracks (squared, spline, and circle track (see Fig. 5) twice in a row with the three models. Since we only gave the starting, turning, and finishing points, the path for each track was slightly different among subjects. With this randomness, we could estimate whether the recognition model was over-fitted. Also, the order of experiments was randomly shuffled for each subject to avoid the effects of fatigue and adaption. The square track consisted of four walking directions (F, B, L, R), and the spline and circle track had only forward walking with turning (F). We designed those tracks to estimate the recognition accuracy and compare the performances of models. Recognition results and mechanical values such as interaction force, torque, and odometry of WANDER were recorded for calculating performance indices (see Section III-D).

2) Sloping Ground Experiments: Subjects walked on a 6 m inclined and declined sloping ground with a 5° (0.087 rd). We used the measured angle itself with the same γ value for all subjects to ensure consistent experimental results. For example, when the subject was walking on an inclining ground with an angle of θ_s radians, the $S(v)$ curve was bent to get lower values (See. Fig. 4. blue curves), and it was the opposite on the declining

ground (See. Fig. 4. red curves). The subject walked on the slope in four different ways: walking forward on the inclining (1) and declining (3) ground, walking backward on the inclining (2) and declining (4) ground. The order of experiments and recorded information were the same as the experiment on the flat ground.

D. Performance Indices

The performance of each parameter variation was validated with three indices and one questionnaire. The first index was the recognition accuracy of human walking patterns. The walking direction recognition neural network was positioned upstream of the variable admittance control within the algorithm architecture. The accuracy of recognition could directly affect the performance of the proposed strategy. The second index was a cumulative absolute impulse (CAI) to assess transparency. It was computed as the integral of the absolute values of force over time as

$$CAI = \int_0^t |F|\, dt + \int_0^t |\tau|\, dt \qquad (13)$$

where F and τ are the interaction force and torque between WANDER and humans and time, and t is time. The assumption is that the total distances are equal. However, if the distance in the comparing experiment differs, we can make compensation using the square root of the distance ratio. We introduced this index because the admittance controller and WANDER act as dampers. Energy-based metrics alone may not capture transparency, especially with oscillations. CAI effectively addresses this, being an impulse-wise index.

The third index was the spectral arc length (η_{sal}) that represents the movement smoothness [26]. η_{sal} was defined as the arc length of the amplitude and frequency-normalized Fourier magnitude spectrum of the force profile ($F(t)$, $t \in [0, T]$) as

$$\eta_{sal} = \int_0^{W_c} \sqrt{\left(\frac{1}{W_c}\right)^2 + \left(\frac{d\hat{F}(w)}{dw}\right)^2}\, dw, \hat{F}(w) = \frac{F(w)}{F(0)} \qquad (14)$$

where $F(w)$ is the Fourier transformed magnitude spectrum of $F(t)$ and it was normalized by $F(0)$ that is the DC component. W_c is the cutoff frequency and is set as 20 Hz being able to cover the human walking movements [27].

The questionnaire was the NASA Task Load Index (NASA-TLX) for qualification analysis based on user responses. All subjects filled it at the end of the experiment of each model. For statistical data analysis, the one-way repeated-measures analysis of variance (ANOVA) was conducted to assess and compare the three different models. These analyses were performed on raw data before normalization to avoid the potential influence of normalization, and the significance level was set to 0.05.

IV. RESULTS

A. Recognition Accuracy

The recognition accuracy was calculated based on the data that was recorded when the subject was walking on the square track during the test session. Since the recognition accuracy on the spline, circle, and sloping track had only one label, F, we extracted the recognition accuracy on the square track, which includes all types of walking patterns. The overall recognition

Fig. 6. Recognition accuracy of human walking. The average accuracy of five classes was 96.1% and its standard deviation was 5.7% from ten subjects.
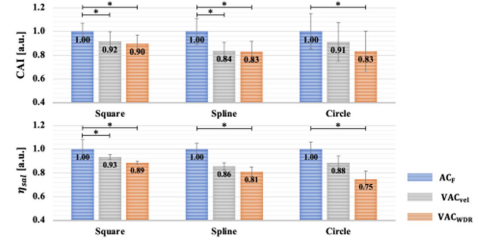

Fig. 7. Experimental result for three types of tracks on the flat ground. CAI and η_{sal} of all models are presented. $*$ stands for $p < 0.05$.

accuracy was 96.1% and its standard deviation was 5.7%. The accuracy for each class is shown in Fig. 6.

B. On the Flat Ground

In Fig. 7, the CAI and the η_{sal} values were normalized by those values of AC_F. On the square track, CAI of the VAC_{vel} and VAC_{WDR} was decreased by 8.32% and 10.24%, respectively, compared to AC_F. η_{sal} was decreased by 6.68% and 11.46%, respectively, and All those reductions showed a statistically significant difference ($p < 0.05$). On the spline and circle track, VAC_{WDR} showed superior performance compared to both VAC_{vel} and AC_F. CAI of VAC_{WDR} and η_{sal} was decreased compared to AC_F (Spline: 16.94% and 19.07%, Circle: 16.55% and 25.37%) with statistically significant differences ($p < 0.05$). The indexes of VAC_{vel} were decreased compared to AC_F, but, it didn't show statistically significant differences except CAI on the spline track. Overall, VAC_{WDR} exhibited superior performance compared to VAC_{vel} across all tracks. Specifically, as VAC_{WDR} adjusted damping via the walking direction and force to reduce oscillations, the η_{sal} values of VAC_{WDR} were lower than those of VAC_{vel}.

C. On the Sloping Ground

In Fig. 8, results are presented for the sloping track with the four types of patterns, i.e., walking forward and backward on the inclining and declining ground. In this case, because the slope adaptive strategy is only able to be implemented based on waking direction recognition, $VAC_{WDR.S}$ and VAC_{WDR} were compared at each pattern. All index values were normalized by those values of VAC_{WDR}. While subjects were walking on the inclining ground, CAI of $VAC_{WDR.S}$ showed lower value than VAC_{WDR} (Forward: -26.88% with statistically significant difference ($p < 0.05$), backward: -9.50%). Subjects walked more slowly when moving backward, resulting in a lower reduction ratio compared to walking forward. on the declining ground, η_{sal} values of $VAC_{WDR.S}$ were lower than

Fig. 8. Result from four walking patterns on the slope. $VAC_{WDR.S}$ showed lower CAI on the inclining ground and lower η_{sal} on the declining ground.
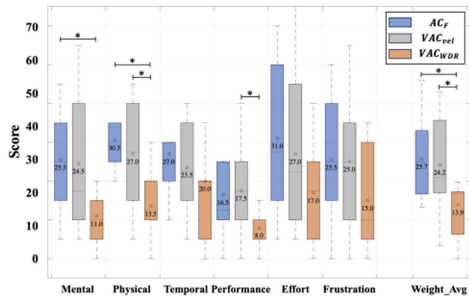

Fig. 9. NASA task load index. $Weight_{Avg}$ was calculated by each user's weighing values of each index. $*$ stands for $p < 0.05$.

VAC_{WDR} (Forward: -7.27%, backward: -15.67% with statistically significant difference ($p < 0.05$)). In the four slope cases, $VAC_{WDR.S}$ adapts with distinct goals: prioritizing safety weight support on declining slopes and enhancing transparency for easier walking on inclines. Therefore, CAI becomes an important index for walking upward, while N_{sal} becomes crucial for walking downward. $VAC_{WDR.S}$ exhibited superior performance in each case through its slope adaptation.

D. Users' Response

The results of the NASA Task Load Index (NASA-TLX) are presented in Fig. 9. VAC_{WDR} obtained high scores in all sub-indexes, notably demonstrating a statistically significant difference ($p < 0.05$) compared to VAC_{vel} in physical demand and performance. The weighted average, representing overall user response, indicated that VAC_{WDR} is superior to the other two models, with a statistically significant difference.

V. DISCUSSION

Based on the experimental validation, we showed that VAC_{WDR} demonstrated superior transparency and movement smoothness compared to AC_F and VAC_{vel} across all tracks. Although the performance difference between VAC_{WDR} and VAC_{vel} was not statistically significant, VAC_{WDR} consistently exhibited higher performance values on average than VAC_{vel}. Notably, The improvement in smoothness may have influenced the NASA-TLX scores, as indicated by subjects assigning higher scores to VAC_{WDR}. The high transparency was achieved by decreasing damping along the same direction of walking. Simultaneously, the high movement smoothness resulted from increasing damping along the perpendicular axis and the opposite direction of walking. The pelvis movement,

not rigidly fixed to the robot, was the source of oscillation, caused by velocity mismatch between human and robot. Adjusting damping parameters, considering walking direction and force, can reduce oscillations. We validated high accuracy in walking direction recognition. Even with varied trajectories, the recognition remained accurate as long as subjects maintained consistent walking direction. We introduced a slope adaptive admittance controller, which adjusts its parameters based on the slope of the ground. Decreasing the controller's parameters on inclines enhances transparency for easier walking while increasing parameters on declines ensures stable walking.

The aim is to create a walking aid robot to substitute therapists, enabling independent rehabilitation and physical activity. This paper focuses on ensuring it can seamlessly track the user's movements and provide assistance when required, not on the weight support. Users can receive partial weight support on declined ground by leaning on the robot, acting as an input force to the controller. Additionally, we can utilize the "Standing" class as a weight support function on both flat and sloped surfaces by either increasing damping or stopping the robot altogether. We acknowledge these avenues as potential areas for further exploration and development.

We presented a vision-based recognition of walking direction. Due to the classification nature of this model, windowing is indispensable to enhance accuracy but may introduce errors when abruptly changing the walking direction. Also, skeletal pose extraction utilized at close observation distances, may not be perfectly accurate, especially in situations involving directional changes. The next objective is to extract the all-direction of walking and real-time control. It will involve the development of a regression-based model, removing the sampling window. In addition, Processing only 2D images for recognition might limit the recognition accuracy. Incorporating 3D images and depth information, along with 3D skeletal pose information, could potentially enhance accuracy. The consideration of depth is crucial because the distance between the human and the camera can vary, and depth information provides vital cues for walking direction recognition. Therefore, leveraging 3D images and depth information could lead to more robust and accurate recognition results.

To address the potential alteration of walking posture due to adaptive parameter updates, we implemented a curve-shaped continuous parameter-varying function. Notably, despite fluctuations in horizontal velocities and corresponding damping updates in spline and circular track scenarios, the recognition accuracy remained highly accurate (worst case: 99.16%). However, it's essential to note that there are possibilities of errors arising from parameter changes and class-switching moments. These factors will be considered in further research. We need to consider the user's comfort perception, especially when the walking state suddenly changes. Increasing damping in opposite and perpendicular directions enhances smoothness and continuous adjustment function based on velocity improves the user's comfort observed by NASA-TLX.

As all subjects are young and healthy, Validation with elderly individuals and patients is essential, as indicated by [28] and [29], who highlighted distinct gait behaviors in these groups, especially in Alzheimer's patients. Understanding these differences in gait patterns and measuring performance variations among these populations is crucial moving forward. In the experiments with eleven subjects of varying physical features, we set initial mass and damping parameters based on an empirical rule.

To generalize further, we recently introduced the Personalizable search algorithm for admittance parameters (referenced as [30]), which facilitates the selection of mass and damping based on the user's preferences. Furthermore, users' characteristics may fluctuate due to various physical conditions, such as feeling relaxed, fatigued, experiencing pain, etc. Exploring the impact of these factors on the performance of the system is a direction for future research.

Building upon human skeletal movement, including the upper body, we aim to enhance assistive performance securely, with a focus on fall prevention. In a previous study [7], instances of falling were identified by monitoring the COP using a cane-type robot, which maintained the COP within a support triangle defined by the feet and robot positions. With access to skeletal data from both the upper and lower body, we can detect unbalanced postures and potential falls earlier. Our objective is to design an assistive balancing mechanism considering overall body movements, and calculating the COM and COP to maintain a safe posture boundary.

VI. CONCLUSION

We introduced a new control strategy for a walking assistive robot, improving transparency and movement smoothness. By analyzing human skeletal movements, we identified five walking patterns and designed a variable admittance controller. We incorporated slope angle measurement to enhance transparency and safety on the slope.

REFERENCES

[1] A. Ghaffar, A. A. Dehghani-Sanij, and S. Q. Xie, "A review of gait disorders in the elderly and neurological patients for robot-assisted training," *Disabil. Rehabil.: Assistive Technol.*, vol. 15, no. 3, pp. 256–270, 2020.

[2] Q. Yan, J. Huang, C. Tao, X. Chen, and W. Xu, "Intelligent mobile walking-aids: Perception, control and safety," *Adv. Robot.*, vol. 34, no. 1, pp. 2–18, 2020.

[3] J. K. Mehr, M. Akbari, P. Faridi, H. Xing, V. K. Mushahwar, and M. Tavakoli, "Artificial-intelligence-powered lower limb assistive devices: Future of home care technologies," *Adv. Intell. Syst.*, vol. 5, 2023, Art. no. 2200361.

[4] C. A. Cifuentes, C. Rodriguez, A. Frizera-Neto, T. F. Bastos-Filho, and R. Carelli, "Multimodal human–robot interaction for walker-assisted gait," *IEEE Syst. J.*, vol. 10, no. 3, pp. 933–943, Sep. 2016.

[5] M. Fernandez-Carmona et al., "Walk-IT: An open-source modular low-cost smart rollator," *Sensors*, vol. 22, no. 6, 2022, Art. no. 2086.

[6] J. Huang, P. Di, T. Fukuda, and T. Matsuno, "Motion control of omni-directional type cane robot based on human intention," in *Proc. IEEE/RSJ Int. Conf. Intell. Robots Syst.*, 2008, pp. 273–278.

[7] P. Di et al., "Fall detection and prevention control using walking-aid cane robot," *IEEE/ASME Trans. Mechatronics*, vol. 21, no. 2, pp. 625–637, Apr. 2016.

[8] G. Aguirre-Ollinger and H. Yu, "Omnidirectional platforms for gait training: Admittance-shaping control for enhanced mobility," *J. Intell. Robot. Syst.*, vol. 101, pp. 1–17, 2021.

[9] D. Marks et al., "The andago for overground gait training in patients with gait disorders after stroke-results from a usability study," *Physiotherapy Res. Rep.*, vol. 2, no. 2, pp. 1–8, 2019.

[10] P. Di, J. Huang, S. Nakagawa, K. Sekiyama, and T. Fukuda, "Fall detection and prevention in the elderly based on the ZMP stability control," in *Proc. IEEE Workshop Adv. Robot. Social Impacts*, 2013, pp. 82–87.

[11] S. Itadera, E. Dean-Leon, J. Nakanishi, Y. Hasegawa, and G. Cheng, "Predictive optimization of assistive force in admittance control-based physical interaction for robotic gait assistance," *IEEE Robot. Automat. Lett.*, vol. 4, no. 4, pp. 3609–3616, Oct. 2019.

[12] J. Huang, W. Xu, S. Mohammed, and Z. Shu, "Posture estimation and human support using wearable sensors and walking-aid robot," *Robot. Auton. Syst.*, vol. 73, pp. 24–43, 2015.

[13] F. J. Ruiz-Ruiz, A. Giammarino, M. Lorenzini, J. M. Gandarias, J. H. Gómez-De-Gabriel, and A. Ajoudani, "Improving standing balance performance through the assistance of a mobile collaborative robot," in *Proc. IEEE Int. Conf. Robot. Automat.*, 2022, pp. 10017–10023.

[14] F. Ferraguti, C. Talignani Landi, L. Sabattini, M. Bonfe, C. Fantuzzi, and C. Secchi, "A variable admittance control strategy for stable physical human–robot interaction," *Int. J. Robot. Res.*, vol. 38, no. 6, pp. 747–765, 2019.

[15] W. Xu, J. Huang, Y. Wang, C. Tao, and L. Cheng, "Reinforcement learning-based shared control for walking-aid robot and its experimental verification," *Adv. Robot.*, vol. 29, no. 22, pp. 1463–1481, 2015.

[16] G. Chalvatzaki, X. S. Papageorgiou, P. Maragos, and C. S. Tzafestas, "Learn to adapt to human walking: A model-based reinforcement learning approach for a robotic assistant rollator," *IEEE Robot. Automat. Lett.*, vol. 4, no. 4, pp. 3774–3781, Oct. 2019.

[17] Y. Aydin, O. Tokatli, V. Patoglu, and C. Basdogan, "Stable physical human-robot interaction using fractional order admittance control," *IEEE Trans. Haptics*, vol. 11, no. 3, pp. 464–475, Jul.–Sep. 2018.

[18] K. Wakita, J. Huang, P. Di, K. Sekiyama, and T. Fukuda, "Human-walking-intention-based motion control of an omnidirectional-type cane robot," *IEEE/ASME Trans. On Mechatronics*, vol. 18, no. 1, pp. 285–296, Feb. 2013.

[19] J. Li, L. Zhao, and T. Li, "Robotic walker for slope mobility assistance with active-passive hybrid actuator," *Chin. J. Mech. Eng.*, vol. 34, no. 1, pp. 1–10, 2021.

[20] M. Schimpl et al., "Association between walking speed and age in healthy, free-living individuals using mobile accelerometry—a cross-sectional study," *PLoS One*, vol. 6, no. 8, 2011, Art. no. e23299.

[21] M. Abadi et al., "Tensorflow: Large-scale machine learning on heterogeneous distributed systems," 2016, *arXiv:1603.04467*.

[22] D. P. Kingma and J. Ba, "Adam: A method for stochastic optimization," 2014, *arXiv:1412.6980*.

[23] F. Ficuciello, L. Villani, and B. Siciliano, "Variable impedance control of redundant manipulators for intuitive human–robot physical interaction," *IEEE Trans. Robot.*, vol. 31, no. 4, pp. 850–863, Aug. 2015.

[24] A. Atrsaei et al., "Gait speed in clinical and daily living assessments in Parkinson's disease patients: Performance versus capacity," *npj Parkinson's Dis.*, vol. 7, no. 1, 2021, Art. no. 24.

[25] S. Itadera and G. Cheng, "Admittance model optimization for gait balance assistance of a robotic walker: Passive model-based mechanical assessment," in *Proc. IEEE Int. Conf. Robot. Automat.*, 2022, pp. 7014–7020.

[26] S. Balasubramanian, A. Melendez-Calderon, and E. Burdet, "A robust and sensitive metric for quantifying movement smoothness," *IEEE Trans. Biomed. Eng.*, vol. 59, no. 8, pp. 2126–2136, Aug. 2012.

[27] J. J. Kavanagh and H. B. Menz, "Accelerometry: A technique for quantifying movement patterns during walking," *Gait Posture*, vol. 28, no. 1, pp. 1–15, 2008.

[28] M. Y. Osoba, A. K. Rao, S. K. Agrawal, and A. K. Lalwani, "Balance and gait in the elderly: A contemporary review," *Laryngoscope Invest. Otolaryngol.*, vol. 4, no. 1, pp. 143–153, 2019.

[29] D. Maquet et al., "Gait analysis in elderly adult patients with mild cognitive impairment and patients with mild Alzheimer's disease: Simple versus dual task: A preliminary report," *Clin. Physiol. Funct. Imag.*, vol. 30, no. 1, pp. 51–56, 2010.

[30] A. Fortuna et al., "A personalizable controller for the walking assistive omni-directional exo-robot (WANDER)," 2024, *arXiv:2405.04359*.